Computers and Fluids 156 (2017) 239–246

Contents lists available at ScienceDirect

Computers and Fluids

journal homepage: www.elsevier.com/locate/compfluid

Conservative Allen–Cahn–Navier–Stokes system for incompressible two-phase fluid flows

Darae Jeong, Junseok Kim*

Department of Mathematics, Korea University, Seoul 02841, Republic of Korea

ARTICLE INFO

Article history:
Received 16 September 2016
Revised 23 May 2017
Accepted 7 July 2017
Available online 8 July 2017

Keywords:
Cahn–Hilliard equation
Conservative Allen–Cahn equation
Phase-field model
Navier–Stokes equation
Interfacial tension
Multigrid method

ABSTRACT

A new phase-field model for immiscible incompressible two-phase liquid flows has been developed. The model consists of a conservative Allen–Cahn equation with a space-time dependent Lagrange multiplier and a modified Navier–Stokes equation. Even though most phase-field methods for the multiphase flows preserve total mass, the bulk phase concentrations tend to shift from equilibrium concentration values of a double-well potential. The proposed model has a good feature which avoids mass spreading to the bulk phases. To validate the new system, the deformation of a drop from the initial circular shape in shear flow is presented and compared with other numerical results.

1. Introduction

Many important industrial problems involve multiphase and multicomponent fluid flows [1]. There are many mathematical models and numerical solution methods for the multiphase and multicomponent fluid flows such as the level set method [1–3], the phase-field method [1,4,5], the immersed boundary method [1,6,7], and the lattice Boltzmann method [8–10], to name a few. In this paper, we focus on the phase-field method. The Cahn–Hilliard (CH) equation [11] has been used in simulating two-phase fluid flows [12–19] and multi-component fluid flows [20], see a review paper [21] and references therein. However, for a long time simulation, the bulk phase concentrations tend to shift from equilibrium concentration values of a double-well potential even though most phase-field methods for the multiphase flows preserve total mass. To overcome this drawback, we propose a new phase-field model for immiscible incompressible two-phase liquid flows. The proposed model consists of a conservative Allen–Cahn equation with a space-time dependent Lagrange multiplier [22,23] and a modified Navier–Stokes equation. The new system has a good feature which avoids mass spreading to the bulk phase. In this paper, we consider the following system modeling viscous, immiscible, incompressible, two-phase fluid flow with surface tension force:

$$\frac{\partial \mathbf{u}}{\partial t} + \mathbf{u}\cdot\nabla\mathbf{u} = -\nabla p + \frac{1}{Re}\Delta\mathbf{u} + \mathbf{F}_s(\phi), \tag{1}$$

$$\nabla\cdot\mathbf{u} = 0, \tag{2}$$

where $\mathbf{u}$ is the fluid velocity, p is the pressure, Re is the Reynolds number, and $\mathbf{F}_s$ is the surface tension of the interface. The interfacial force $\mathbf{F}_s(\phi)$ is given as

$$\mathbf{F}_s(\phi) = -\frac{3\sqrt{2}\epsilon}{4We}\nabla\cdot\left(\frac{\nabla\phi}{|\nabla\phi|}\right)|\nabla\phi|\nabla\phi,$$

where We is the Weber number [17]. The governing equation of the order parameter ϕ is given by the following phase-field equation:

$$\frac{\partial \phi}{\partial t} + \nabla\cdot(\phi\mathbf{u}) = \frac{1}{Pe}(-F'(\phi) + \epsilon^2\Delta\phi) + \beta(t)\sqrt{F(\phi)}, \tag{3}$$

where Pe is the Peclet number, $F(\phi) = 0.25(\phi^2-1)^2$, ϵ is a positive constant, and $\beta(t)$ is a non-constant Lagrange multiplier which enforces the mass conservation. Note that we view the current model as a computational method for simulating viscous, immiscible, incompressible, two-phase fluid flow with surface tension and gravitational forces.

If $\beta(t)\sqrt{F(\phi)}$ is absent in Eq. (3), then the equation becomes a convective Allen–Cahn equation and the rigorous mathematical analysis for the resulting Allen–Cahn–Navier–Stokes system was extensively covered in [24]. Yang et al. [19] employed the following

* Corresponding author.
E-mail addresses: cfdkim@korea.ac.kr, tinayoyo@korea.ac.kr (J. Kim).
URL: http://math.korea.ac.kr/~cfdkim (J. Kim)

http://dx.doi.org/10.1016/j.compfluid.2017.07.009
0045-7930/

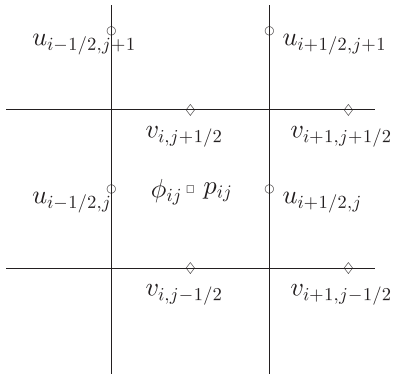

Fig. 1. MAC discretization of the velocity, pressure, and phase-field components.

energetic variational phase-field method to simulate jet pinching-off and drop formation:

$$\frac{\partial \phi}{\partial t} + \nabla \cdot (\phi \mathbf{u}) = \frac{1}{Pe}(-F'(\phi) + \epsilon^2 \Delta \phi) + \beta(t). \tag{4}$$

Di et al. [25] presented an adaptive moving mesh algorithm for meshes of unstructured polyhedra in three space dimensions using a conservative Allen–Cahn–Navier–Stokes system. Shah and Yuan [5] proposed an artificial compressibility based numerical method for a phase field model for simulating two-phase incompressible viscous flows. In [26], the authors have introduced a globally conservative residual-based Allen–Cahn phase field stabilized finite element model for the simulation of two immiscible fluids using the same Eq. (4). Using the conservative Allen–Cahn equation, the authors in [8,9] proposed and improved a conservative Boltzmann method to track the interface between two different fluids. The method conserves mass locally and globally.

The remaining parts of this paper are organized as follows. In Section 2, we give the numerical solution algorithm. To validate the new proposed model, a droplet deformation in shear flow is presented in Section 3. In Section 4, conclusions are drawn.

2. Numerical solutions

The proposed numerical method is composed of two parts: A projection method for the modified Navier–Stokes equation [27] and a hybrid method for the conservative Allen–Cahn equation with a space-time dependent Lagrange multiplier [23]. Let $\Omega = (a, b) \times (c, d)$ be a computational domain, which is partitioned into a uniform mesh with a constant mesh spacing $h = (b-a)/N_x = (d-c)/N_y$, where N_x and N_y are the numbers of cells in x- and y- directions, respectively. For $i = 1, \cdots, N_x$ and $j = 1, \cdots, N_y$, let $(x_i, y_j) = (a + (i - 0.5)h, c + (j - 0.5)h)$ be the cell centers. Let ϕ_{ij}^n and p_{ij}^n be approximations of $\phi(x_i, y_j, n\Delta t)$ and $p(x_i, y_j, n\Delta t)$, respectively, where $\Delta t = T/N_t$ is the temporal step size, T is the final time, and N_t is the total number of time steps. Velocities $u_{i+\frac{1}{2},j}$ and $v_{i,j+\frac{1}{2}}$ are defined at cell edges $(x_{i+\frac{1}{2}}, y_j) = (a + ih, c + (j - 0.5)h)$ and $(x_i, y_{j+\frac{1}{2}}) = (a + (i - 0.5)h, c + jh)$, respectively. The staggered marker-and-cell (MAC) mesh is used [28]. In the MAC mesh, pressure and phase fields are defined at centers and velocities are at edges (see Fig. 1).

Given $\mathbf{u}^n$, and ϕ^n, we want to find $\mathbf{u}^{n+1}$, ϕ^{n+1}, and p^{n+1} which solve Eqs. (1)–(3). Initialize $\mathbf{u}^0$ to be the divergence-free velocity field and ϕ^0 to be the locally equilibrated concentration profile.

Step 1. Solve the intermediate velocity field $\tilde{\mathbf{u}}$:

$$\frac{\tilde{\mathbf{u}} - \mathbf{u}^n}{\Delta t} = \frac{1}{Re}\Delta_d \mathbf{u}^n + \mathbf{F}_s^n - (\mathbf{u} \cdot \nabla_d \mathbf{u})^n,$$

where discretizations of the surface tension force $\mathbf{F}_s^n$ and the advection term can be found in [17,29]. For the discrete Laplacian operator Δ_d, we use the standard five-point discretization. For example, $\Delta_d u_{i+\frac{1}{2},j} = (u_{i-\frac{1}{2},j} + u_{i+\frac{3}{2},j} - 4u_{i+\frac{1}{2},j} + u_{i+\frac{1}{2},j-1} + u_{i+\frac{1}{2},j+1})/h^2$. Next, we solve Eqs. (5) and (6) for the pressure field at $(n+1)$ time level.

$$\frac{\mathbf{u}^{n+1} - \tilde{\mathbf{u}}}{\Delta t} = -\nabla_d p^{n+1}, \tag{5}$$

$$\nabla_d \cdot \mathbf{u}^{n+1} = 0. \tag{6}$$

After taking the divergence operator to Eq. (5) and using Eq. (6), we have the following Poisson equation.

$$\Delta_d p^{n+1} = \frac{1}{\Delta t}\nabla_d \cdot \tilde{\mathbf{u}}. \tag{7}$$

The resulting linear system of Eq. (7) is solved using a multigrid method [30].

Step 2. Update the phase-field from ϕ^n *to* ϕ^{n+1}: To solve Eq. (3), we use an operator splitting method, in which the original problem is split into a sequence of simpler problems [23]:

$$\frac{\partial \phi}{\partial t} = \frac{\epsilon^2}{Pe}\Delta \phi - \nabla \cdot (\phi \mathbf{u}), \tag{8}$$

$$\frac{\partial \phi}{\partial t} = -\frac{F'(\phi)}{Pe}, \tag{9}$$

$$\frac{\partial \phi}{\partial t} = \beta(t)\sqrt{F(\phi)}. \tag{10}$$

First, we solve Eq. (8) by a semi-implicit scheme:

$$\frac{\phi_{ij}^* - \phi_{ij}^n}{\Delta t} = \frac{\epsilon^2}{Pe}\Delta_d \phi_{ij}^* - \nabla_d \cdot (\phi \mathbf{u})_{ij}^n. \tag{11}$$

We use the multigrid method [30] to solve the implicit discrete Eq. (11). Next, we solve Eq. (9) analytically using the method of separation of variables

$$\phi_{ij}^{**} = \frac{\phi_{ij}^*}{\sqrt{e^{-\frac{2\Delta t}{Pe}} + (\phi_{ij}^*)^2(1 - e^{-\frac{2\Delta t}{Pe}})}}. \tag{12}$$

Eq. (10) is discretized as

$$\frac{\phi_{ij}^{n+1} - \phi_{ij}^{**}}{\Delta t} = \beta^{**}\sqrt{F(\phi_{ij}^{**})}. \tag{13}$$

Using Eq. (13) and the mass conservation, we have

$$\sum_{i=1}^{N_x}\sum_{j=1}^{N_y}\phi_{ij}^0 = \sum_{i=1}^{N_x}\sum_{j=1}^{N_y}\phi_{ij}^{n+1} = \sum_{i=1}^{N_x}\sum_{j=1}^{N_y}\left(\phi_{ij}^{**} + \Delta t\beta^{**}\sqrt{F(\phi_{ij}^{**})}\right). \tag{14}$$

Thus,

$$\beta^{**} = \frac{1}{\Delta t}\sum_{i=1}^{N_x}\sum_{j=1}^{N_y}(\phi_{ij}^0 - \phi_{ij}^{**}) \Big/ \sum_{i=1}^{N_x}\sum_{j=1}^{N_y}\sqrt{F(\phi_{ij}^{**})}. \tag{15}$$

Finally, we get ϕ^{n+1} from Eq. (13), i.e., $\phi_{ij}^{n+1} = \phi_{ij}^{**} + \Delta t\beta^{**}\sqrt{F(\phi_{ij}^{**})}$. Note that here we focus on the conservative Allen–Cahn–Navier–Stokes system for incompressible two-phase fluid flows and we use first-order numerical schemes. However, we can use high-order numerical schemes [19,31] for the governing equations.

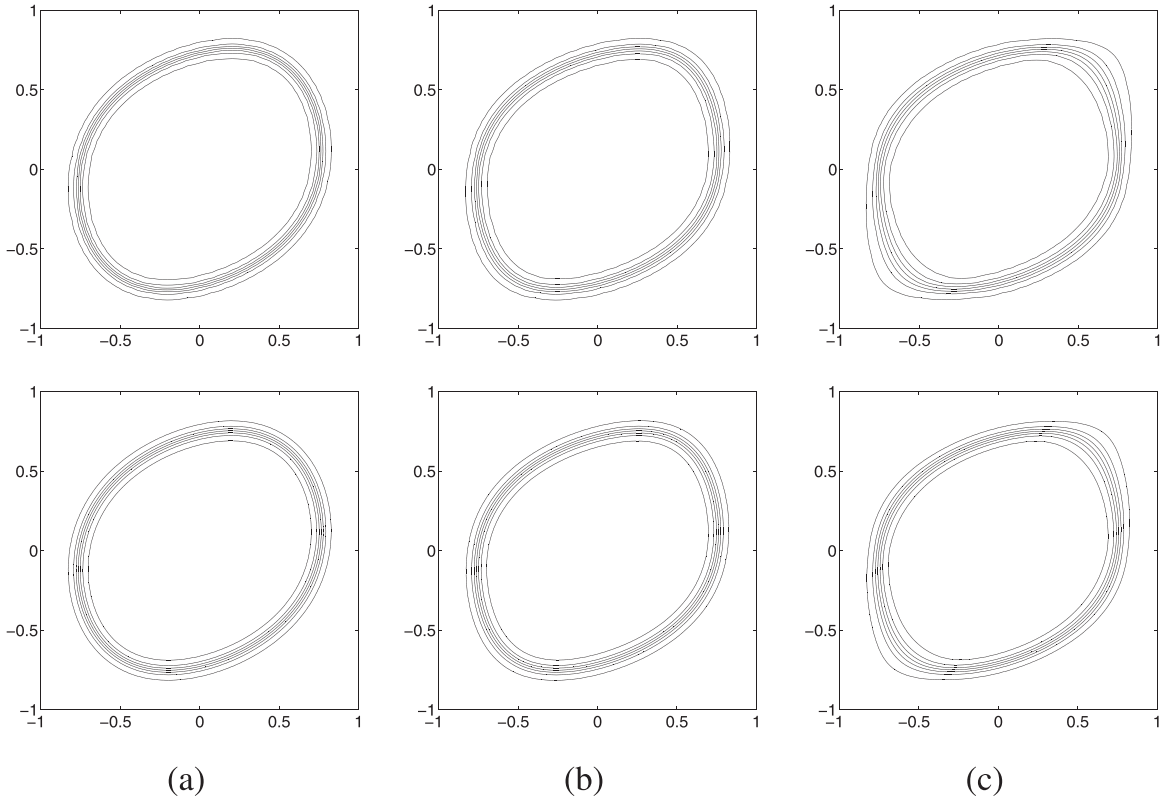

Fig. 2. The effect of Peclet number. (a) $Pe = 0.01$, (b) $Pe = 0.1$, and (c) $Pe = 1$. Contour levels are $-0.9, -0.6, -0.3, 0, 0.3, 0.6, 0.9$. Top and bottom rows are results with ϵ_4, $h = 1/32$, $\Delta t = 0.1h^2Re$ and ϵ_8, $h = 1/64$, $\Delta t = 0.1h^2Re$, respectively.

3. Numerical experiment

To demonstrate the performance of the proposed conservative Allen–Cahn–Navier–Stokes (CAC–NS) system for incompressible two-phase fluid flows, we consider a droplet deformation under shear flow. The initial conditions are a circular droplet and zero velocities on the computational domain $\Omega = (-2, 2) \times (-1, 1)$:

$$\phi(x, y, 0) = \tanh\left(\frac{0.75 - \sqrt{x^2 + y^2}}{\sqrt{2}\epsilon}\right), \quad u(x, y, 0) = v(x, y, 0) = 0.$$

For the top and bottom wall boundary conditions, we take the following:

$$u(x, 1, t) = -u(x, -1, t) = 1, \quad v(x, 1, t) = v(x, -1, t) = 0,$$
$$p_y(x, 1, t) = p_y(x, -1, t) = \phi_y(x, 1, t) = \phi_y(x, -1, t) = 0.$$

We impose the periodic boundary condition for the x-direction for all fields. Across interfacial transition layer ϕ varies from -0.9 to 0.9 over a length of about $2\sqrt{2}\epsilon \tanh^{-1}(0.9)$. Therefore, if we want this value to be about hm, then $\epsilon = \epsilon_m = hm/[2\sqrt{2}\tanh^{-1}(0.9)]$ [21].

3.1. Peclet number effect

As a first test, we investigate the effect of the Peclet number in the model (3). We perform a series of tests with various Peclet numbers with $Re = 10$ and $We = 3$. Fig. 2(a)–(c) show snapshots at time $t = 0.244140625$ with $Pe = 0.01$, $Pe = 0.1$, and $Pe = 1$, respectively. Top and bottom rows are results with ϵ_4, $h = 1/32$, $\Delta t = 0.1h^2Re$ and ϵ_8, $h = 1/64$, $\Delta t = 0.1h^2Re$, respectively. Here, we fixed the model parameters and changed the numerical parameters. We can observe the convergence of the results with refined discretization parameters. If Pe is too small, then the conservative Allen–Cahn dynamics dominates. On the other hand, if Pe is too large, then the interfacial transition layer is not locally equilibrated and the thickness of the layer is not uniform.

3.2. Convergence test

In this section, we investigate the spatial and temporal convergence of the proposed numerical scheme. In this test, we fix the model parameters: $\epsilon = 0.05$, $Re = 100$, and $We = 100$. The initial conditions are a circular droplet and the Couette flow velocities on the computational domain $\Omega = (-2, 2) \times (-1, 1)$:

$$\phi(x, y, 0) = \tanh\left(\frac{0.7 - \sqrt{x^2 + y^2}}{\sqrt{2}\epsilon}\right), \quad u(x, y, 0) = y, \quad v(x, y, 0) = 0.$$

Since there is no closed-form analytic solution for this problem, we consider a reference numerical solution, ϕ^{ref}, which is obtained with very fine spatial and temporal steps. Then, we denote the error by $e_{N_x \times N_y} := \phi_{N_x \times N_y} - \phi^{\text{ref}}$, where $\phi_{N_x \times N_y}$ is the numerical solution on the mesh grid point, $N_x \times N_y$. The convergence rate is defined as the ratio of successive errors, $\log_2(\|e_{N_x \times N_y}\|_2 / \|e_{N_x/2 \times N_y/2}\|_2)$. Here, $\|e_{N_x \times N_y}\|_2$ is measured by the discrete l_2-norm. To verify the convergence of numerical solution with respect to spatial grid, we compute the numerical solutions on the mesh grids with $N_x \times N_y = 2^{n+1} \times 2^n$ for $n = 4, 5, 6$ and 7. In all cases, we use the time step size $\Delta t = 1.0\text{e}{-3}$ and the total time $T = 3$. The reference solution is evaluated with $N_x \times N_y = 512 \times 256$ and $\Delta t = 1.0\text{e}{-3}$. We measure the error between the reference solution and the numerical solution on each grid by using the bilinear interpolation. Table 1 lists the discrete l_2-norm of errors and convergence rates with respect to different spatial step sizes. The results suggest that the proposed numerical method is greater than the first-order accurate in space.

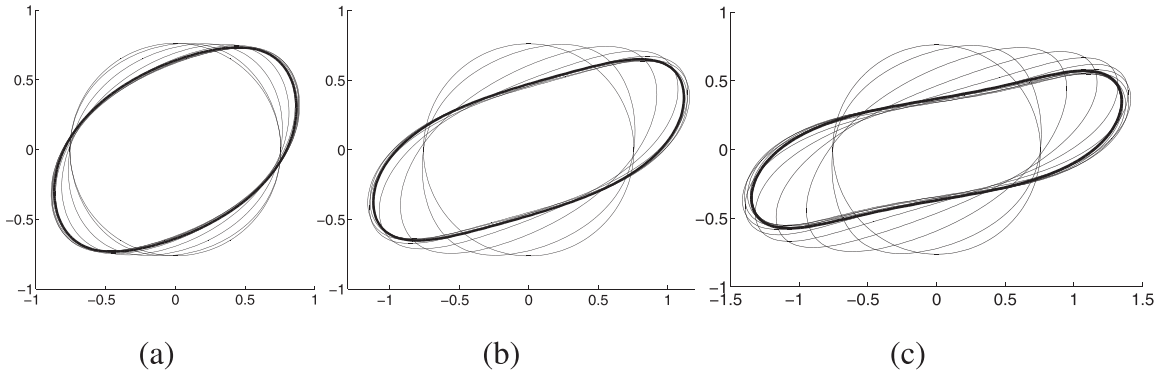

Fig. 3. The effect of capillary number. (a) $Ca = 0.1$, (b) $Ca = 0.2$, and (c) $Ca = 0.3$.

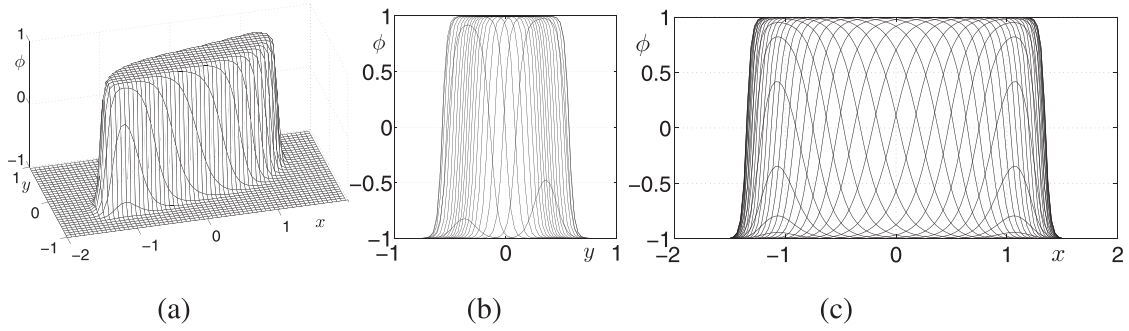

Fig. 4. $Ca = 0.3$ case. (a) Mesh view, (b) cross sections normal to x-axis, and (c) cross sections normal to y-axis.

Table 1
Convergence test with respect to spatial step size.

$N_x \times N_y$	32×16	Rate	64×32	Rate	128×64	Rate	256×128
$\|e_{N_x \times N_y}\|_2$	0.1198	2.6873	0.0186	1.9274	0.0049	1.7236	0.0015

Table 2
Convergence test with respect to time step size.

Δt	0.008	Rate	0.004	Rate	0.002	Rate	0.001
$\|e_{128 \times 64}\|_2$	0.0067	1.0939	0.0031	1.2196	0.0013	1.5836	0.0004

Now, we investigate the accuracy of numerical solution with respect to time step size. For this, we consider the four different time step sizes $\Delta t = 0.008/2^n$ for $n = 0, 1, 2$, and 3. The numerical solution is solved up to time $T = 4$. In all tests, we use the mesh grid $N_x \times N_y = 128 \times 64$. The reference solution ϕ^{ref} is set by the numerical solution with $\Delta t = 0.0005$. Table 2 represents the discrete l_2-norm of errors and convergence rates with respect to different time step sizes. We can see that the rate of convergence is first-order.

We note that we could use high-order schemes to increase the accuracy of the proposed method. However, we focus on the model itself in this paper.

3.3. Capillary number effect

Next, we study the capillary number effect on the droplet deformation. We vary the capillary number $Ca = We/Re$ by changing the We number. The other values of the parameters are the same to the previous test with $Pe = 0.1$. Fig. 3(a)–(c) show the temporal evolution the droplet interface (zero level set) with $Ca = 0.1$, $Ca = 0.2$, and $Ca = 0.3$, respectively. The thick line is the numerical equilibrium profile.

Fig. 4(a)–(c) show mesh view, cross sections normal to x-axis, and cross sections normal to y-axis, respectively, for $Ca = 0.3$ case. We can clearly observe the values of concentration away from the interfacial transition layer are almost equilibrium states, i.e., $\phi \approx \pm 1$.

3.4. Area preservation

There are many benchmark problems relating interface deformation such as diagonal motion of a circular interface, Zalesak's rotating disk, circular interface in shear flow and in a deformation field [8]. In this work, we choose a droplet deformation under a simple shear flow and diagonal motion of a circular interface. We perform the area preservation from the proposed numerical scheme. Here, area is defined as the enclosed region by the zero level set of the phase-field ϕ. In general, $\int_\Omega \phi(x, y, t)dxdy$ is constant, however, $\int_\Omega H(\phi(x, y, t))dxdy$ is not constant with respect to time, where $H(\phi)$ is a heaviside function which is one if $\phi \geq 0$ and is zero otherwise. We define the total mass, $m(\phi)$ and the polygonal area, $A(\phi)$ as

$$m(\phi) = \sum_{i=1}^{N_x} \sum_{j=1}^{N_y} \phi_{ij} h^2 \quad \text{and} \quad A(\phi) = \left| \sum_{l=1}^{M} (X_l Y_{l+1} - Y_l X_{l+1})/2 \right|.$$

Here $\mathbf{X}_l = (X_l, Y_l)$ for $l = 1, \ldots, M$ are the points which are located on the zero level of ϕ and $\mathbf{X}_{M+1} = \mathbf{X}_1$ (see Fig. 5).

Fig. 6 shows temporal evolution of the relative percent error of the polygonal area, $100|A(\phi^n)/A(\phi^0) - 1|$ %, with temporal and spatial step refinements, i.e., $h = 1/32$, $1/64$, and $1/128$ until $t = 19.53125$. Here, we took $Ca = 0.3$ case with $Pe = 0.1$. The relative percent errors are about 0.1% for $h = 1/128$. The inscribed small figures are the zero level contours of the phase-field at the indicated times.

Next, we consider the motion of a circular interface due to a constant velocity field $(u, v) = (1, 1)$ on a doubly periodic

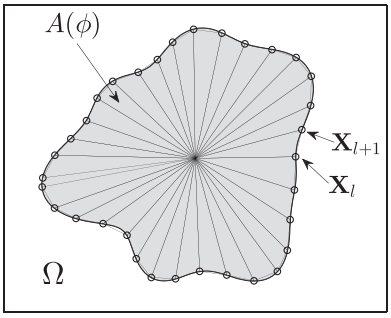

Fig. 5. Polygonal area $A(\phi)$ with the boundary points $\mathbf{X}_l = (X_l, Y_l)$, which are located on the zero level of the phase field, i.e., $A(\phi) = \left|\sum_{l=1}^{M}(X_l Y_{l+1} - Y_l X_{l+1})/2\right|$.

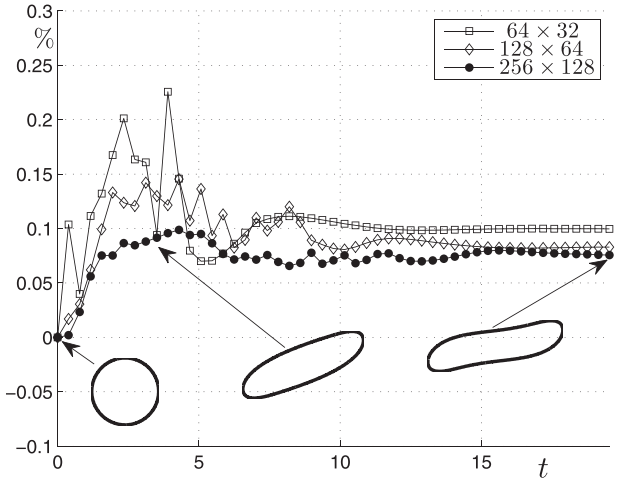

Fig. 6. Temporal evolution of the relative percent error of the polygonal area under shear flow: $100|A(\phi^n)/A(\phi^0) - 1|$ %.

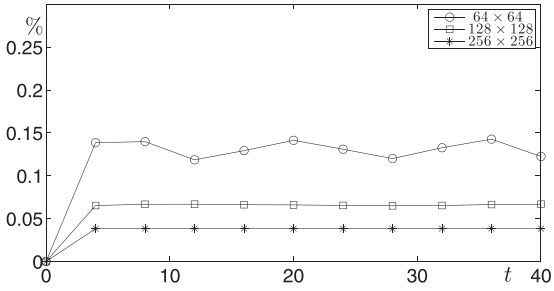

Fig. 7. Temporal evolution of the relative percent error of the polygonal area under diagonal translation: $100|A(\phi^n)/A(\phi^0) - 1|$ %.

computational domain $\Omega = (-2, 2) \times (-2, 2)$ [8]. The initial condition is

$$\phi(x, y, 0) = \tanh\left(\frac{1 - \sqrt{x^2 + y^2}}{\sqrt{2}\epsilon}\right).$$

Here, $\epsilon = 0.1$, $Pe = 0.1$, and $\Delta t = 0.512h$ are used. Fig. 7 shows the temporal evolution of the relative percent error of the polygonal area under diagonal translation, $100|A(\phi^n)/A(\phi^0) - 1|$ %, for three different mess grid points until 10 cycles. We can observe the convergence of the results with refined discretization parameters.

3.5. Comparison with the previous result [32]

Fig. 8 shows the temporal evolution of the drop deformation parameter $D = (L - B)/(L + B)$, where L and B are the maximum and minimum drop lengths, respectively, for $Re = 1$ and several

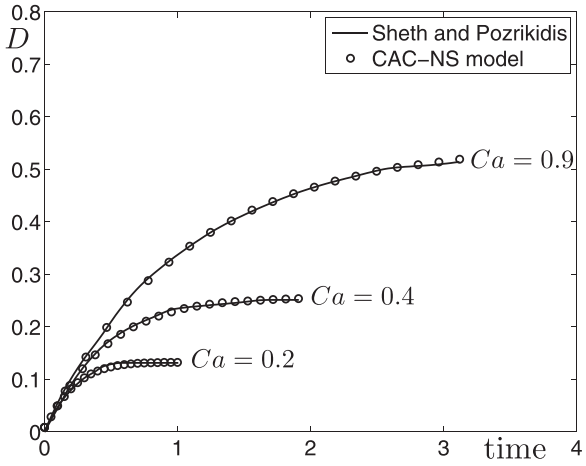

Fig. 8. Temporal evolution of the drop deformation, $D = (L - B)/(L + B)$, for $Re = 1$, $Ca = 0.2,\ 0.4,\ 0.9$.

values of the capillary number. The initial conditions are a circular droplet and the Couette flow velocities on the domain $\Omega = (-1, 1) \times (-1, 1)$:

$$\phi(x, y, 0) = \tanh\left(\frac{0.5 - \sqrt{x^2 + y^2}}{\sqrt{2}\epsilon}\right),\ u(x, y, 0) = y,\ v(x, y, 0) = 0.$$

The parameters used are $h = 1/32$ and $\Delta t = 0.2h^2 Re$. In Fig. 8, the solid line is from Sheth and Pozrikidis [32] and the circled symbol is from the proposed CAC–NS model. They are in good agreement. Here, $Pe = 0.03$, $Pe = 0.06$, and $Pe = 0.135$ are used for $Ca = 0.2$, $Ca = 0.4$, and $Ca = 0.9$, respectively. We can observe that Pe number is proportional to Ca number.

3.6. Comparison with another surface tension model

In this section, we compare the effects of using the present surface tension with a widely adopted surface tension model [25],

$$-\frac{3\sqrt{2}\epsilon}{4We}\nabla \cdot (\nabla\phi \otimes \nabla\phi), \tag{16}$$

where $\nabla\phi \otimes \nabla\phi$ is the tensor product. Eq. (16) is explicitly written as

$$\begin{aligned}\nabla \cdot (\nabla\phi \otimes \nabla\phi) &= \nabla \cdot \begin{pmatrix} \phi_x^2 & \phi_x\phi_y \\ \phi_y\phi_x & \phi_y^2 \end{pmatrix} \\ &= (2\phi_x\phi_{xx} + \phi_y\phi_{xy} + \phi_x\phi_{yy},\ \phi_x\phi_{xy} + \phi_y\phi_{xx} + 2\phi_y\phi_{yy}),\end{aligned} \tag{17}$$

where we omitted the constant coefficient for simplicity. We discretize Eq. (17) using a centered difference scheme.

$$\begin{aligned}&[\nabla \cdot (\nabla\phi \otimes \nabla\phi)]_{ij} \\ &= \Big(\frac{1}{h^3}(\phi_{i+1,j} - \phi_{i-1,j})(\phi_{i+1,j} - 2\phi_{ij} + \phi_{i-1,j}) \\ &\quad + \frac{1}{8h^3}(\phi_{i,j+1} - \phi_{i,j-1})(\phi_{i+1,j+1} + \phi_{i-1,j-1} - \phi_{i+1,j-1} - \phi_{i-1,j+1}), \\ &\quad + \frac{1}{2h^3}(\phi_{i+1,j} - \phi_{i-1,j})(\phi_{i,j+1} - 2\phi_{ij} + \phi_{i,j-1}), \\ &\quad \frac{1}{8h^3}(\phi_{i+1,j} - \phi_{i-1,j})(\phi_{i+1,j+1} + \phi_{i-1,j-1} - \phi_{i+1,j-1} - \phi_{i-1,j+1}) \\ &\quad + \frac{1}{2h^3}(\phi_{i,j+1} - \phi_{i,j-1})(\phi_{i+1,j} - 2\phi_{ij} + \phi_{i-1,j}) \\ &\quad + \frac{1}{h^3}(\phi_{i,j+1} - \phi_{i,j-1})(\phi_{i,j+1} - 2\phi_{ij} + \phi_{i,j-1})\Big)\end{aligned} \tag{18}$$

Let us consider the evolution of a droplet placed within another fluid under shear flow. The initial condition on $\Omega = (-2, 2) \times$

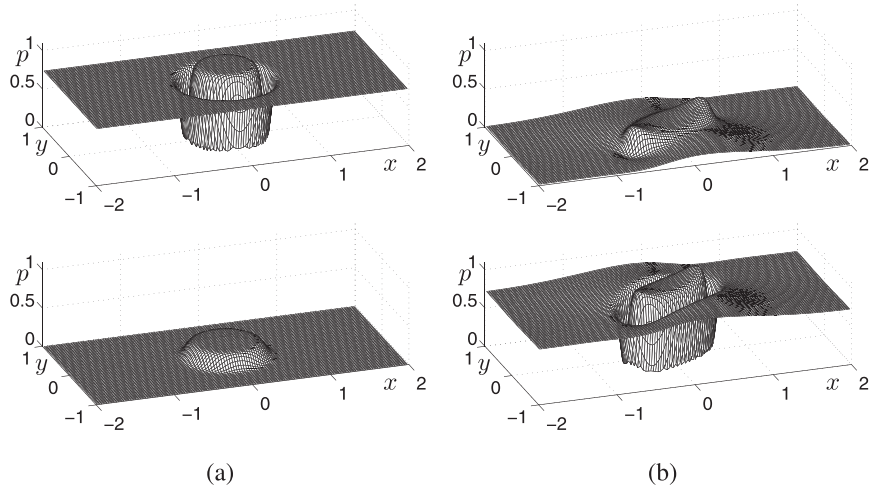

Fig. 9. (a) and (b) are pressure fields after one time step and 5000 time steps, respectively. Top and bottom rows are the results with $-\frac{3\sqrt{2}\epsilon}{4We}\nabla\cdot(\nabla\phi\otimes\nabla\phi)$ and $-\frac{3\sqrt{2}\epsilon}{4We}\nabla\cdot\left(\frac{\nabla\phi}{|\nabla\phi|}\right)|\nabla\phi|\nabla\phi$, respectively.

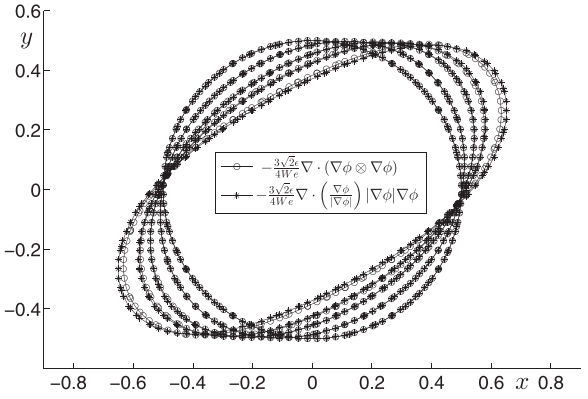

Fig. 10. Temporal evolution of a droplet under a shear flow with two different surface tension models.

$(-1, 1)$ is given as

$$\phi(x,y,0)=\tanh\left(\frac{0.5-\sqrt{x^2+y^2}}{\sqrt{2}\epsilon_8}\right),\quad u(x,y,0)=v(x,y,0)=0.$$

Here, ϵ_8, $Re=20$, $We=10$, $Pe=0.1$, $h=1/32$, and $\Delta t=0.1h^2Re$ are used. In Fig. 9, columns (a) and (b) are the pressure fields after one time step and 5000 time steps, respectively. Top and bottom rows are the results with the surface tension forces $-\frac{3\sqrt{2}\epsilon}{4We}\nabla\cdot(\nabla\phi\otimes\nabla\phi)$ and $-\frac{3\sqrt{2}\epsilon}{4We}\nabla\cdot\left(\frac{\nabla\phi}{|\nabla\phi|}\right)|\nabla\phi|\nabla\phi$, respectively.

Fig. 10 shows the temporal evolution of a droplet under a shear flow with two different surface tension models. In early times, both the results are identical. However, in later times, there is difference.

3.7. Bubble rising test with large density ratio

In this section, we simulate the rising bubble in water with a density ratio of 1000 and viscosity ratio of 100 [33] by the proposed method. The schematic illustration of this test is depicted in Fig. 11. A gas bubble with radius $R=0.5$ is placed at (1, 1) in a rectangular domain $\Omega=[0,2]\times[0,4]$. The density and viscosity of the bubble and the surrounding fluid are noted as ρ_L, μ_L, ρ_H, and μ_H, respectively. Here, we set $h=1/32$, $\Delta t=0.0001$, $T=4$, $Re=35$, $We=125$, $Fr=1$, $\rho_L=1$, $\rho_H=1000$, $\mu_L=1$, and $\mu_H=100$.

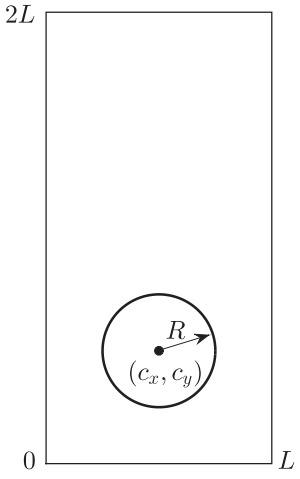

Fig. 11. Schematic illustration of the gas bubble rising in liquid.

The governing equations for variable density and viscosity are as follows:

$$\rho(\phi)(\mathbf{u}_t+\mathbf{u}\cdot\nabla\mathbf{u})=-\nabla p+\frac{1}{Re}\nabla\cdot\left[\eta(\phi)(\nabla\mathbf{u}+\nabla\mathbf{u}^T)\right]+\mathbf{F}_s(\phi)+\frac{\rho(\phi)}{Fr}\mathbf{g},\tag{19}$$

$$\nabla\cdot\mathbf{u}=0,\tag{20}$$

$$\phi_t+\nabla\cdot(\phi\mathbf{u})=\frac{1}{Pe}\left(-F'(\phi)+\epsilon^2\Delta\phi\right)+\beta(t)\sqrt{F(\phi)},\tag{21}$$

where $\rho(\phi)=\rho_H(1-\phi)/2+\rho_L(1+\phi)/2$ is the density, $\eta(\phi)=\eta_H(1-\phi)/2+\eta_L(1+\phi)/2$ is the viscosity, $\mathbf{g}=(0,-1)$ is the gravity.

Then, we obtain the following temporal discretization of dimensionless form of Eqs. (19)–(21) and then we solve these equations in order:

$$\rho^n\frac{\mathbf{u}^{n+1}-\mathbf{u}^n}{\Delta t}=-\rho^n(\mathbf{u}\cdot\nabla_d\mathbf{u})^n-\nabla_d p^{n+1}+\frac{1}{Re}\nabla\cdot\left[\eta(\phi^n)(\nabla_d\mathbf{u}^n+\nabla_d(\mathbf{u}^n)^T)\right]+\mathbf{F}_s^n+\frac{\rho^n}{Fr}\mathbf{g},\tag{22}$$

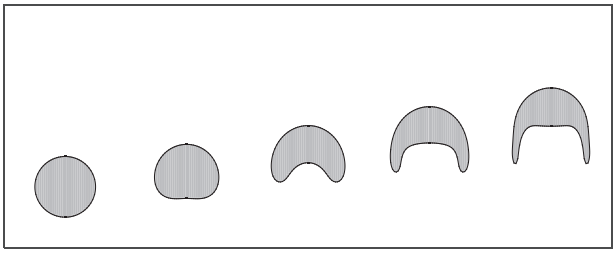

Fig. 12. Time evolution of a bubble rising in liquid at $t = 0, 1, 2, 3,$ and 4.

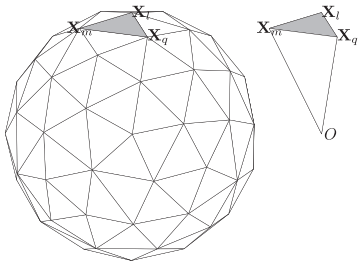

Fig. 13. Schematic illustration for the polyhedron and a tetrahedron with a reference point **O**.

$$\nabla_d \cdot \mathbf{u}^{n+1} = 0, \tag{23}$$

$$\frac{\phi^* - \phi^n}{\Delta t} = \frac{\epsilon^2}{Pe}\Delta_d \phi^* - \nabla_d \cdot (\phi \mathbf{u})^n, \tag{24}$$

$$\phi^{**} = \frac{\phi^*}{\sqrt{e^{-\frac{2\Delta t}{Pe}} + (\phi^*)^2(1 - e^{-\frac{2\Delta t}{Pe}})}}, \tag{25}$$

$$\frac{\phi^{n+1} - \phi^{**}}{\Delta t} = \beta^{**}\sqrt{F(\phi^{**})}. \tag{26}$$

Here, $\beta^{**} = \frac{1}{\Delta t}\sum_{i=1}^{N_x}\sum_{j=1}^{N_y}(\phi_{ij}^0 - \phi_{ij}^{**}) \Big/ \sum_{i=1}^{N_x}\sum_{j=1}^{N_y}\sqrt{F(\phi_{ij}^{**})}$. Fig. 12 shows the temporal evolution of a bubble rising in liquid at $t = 0, 1, 2, 3,$ and 4. We can see that the result is comparable to the result in Ref. [34].

3.8. Comparison study of the Cahn–Hilliard and conservative Allen–Cahn equations

In this section, we show the superiority of the conservative Allen–Cahn (CAC) model compared to the Cahn–Hilliard (CH) model in the case of a single drop with relatively coarse grid points. The CH equation [11,21] is

$$\frac{\partial \phi}{\partial t} = \Delta\left(F'(\phi) - \epsilon^2 \Delta \phi\right). \tag{27}$$

We check the temporal evolution of the discrete volume of a drop without fluid flow. Here, the discrete volume is defined by the total volume of the polyhedrons:

$$V(\mathbf{X}) = \frac{1}{6}\sum_{s=1}^{M_T}[X_q(Y_l Z_m - Y_m Z_l) - Y_q(X_l Z_m - X_m Z_l) + Z_q(X_l Y_m - X_m Y_l)],$$

where M_T is the number of surface triangles $\mathbf{Tri}_s = (\mathbf{X}_l, \mathbf{X}_m, \mathbf{X}_q)$ with a reference point **O** as shown in Fig. 13. Each point $\mathbf{X}_i$ means (X_i, Y_i, Z_i) [35].

The initial droplet is defined to be a spherical shape with radius $R = 0.4$ which is centered at (0.5, 0.5, 0.5) in a three-dimensional domain $\Omega = (0, 1)^3$. For numerical test, we use the following parameters: $Pe = 1$, $\epsilon = 4h/(2\sqrt{2}\tanh^{-1}(0.9))$, $\Delta t = 0.1h^2$, and $T = 10000/2^{12}$. Fig. 14(a) and (b) show the temporal evolution of normalized discrete volume of a droplet in the absence of fluid flow with CH and CAC model when $N_x = N_y = N_z = 32$ and $N_x = N_y = N_z = 64$, respectively. As shown in Fig. 14, although physics of CH model have the mass conservation, the lack of mesh resolution generates the loss of the discrete mass. However, the CAC model conserves the discrete mass regardless of the grid size h.

4. Conclusions

In this paper, we proposed a conservative Allen–Cahn equation with a space-time dependent Lagrange multiplier and a modified Navier–Stokes equation for immiscible incompressible two-phase liquid flows. In the phase-field method for two-phase fluid flows, preservation of total mass is one thing, and preservation of enclosed area (volume) by a contour (isosurface) is another. The new conservative Allen–Cahn–Navier–Stokes system has a good feature preserving enclosed area (volume) under fluid flow deformation. Numerical results confirmed that the proposed method has a good area and volume conservation property. The new scheme will be useful in modeling and simulation three-dimensional drop deformation because it needs relatively coarse grid resolution compared to the standard Cahn–Hilliard–Navier–Stokes system. Further improvements are possible by using higher-order numerical schemes. Another future research direction would be extensions to multi-component (more than two-phase) fluid systems.

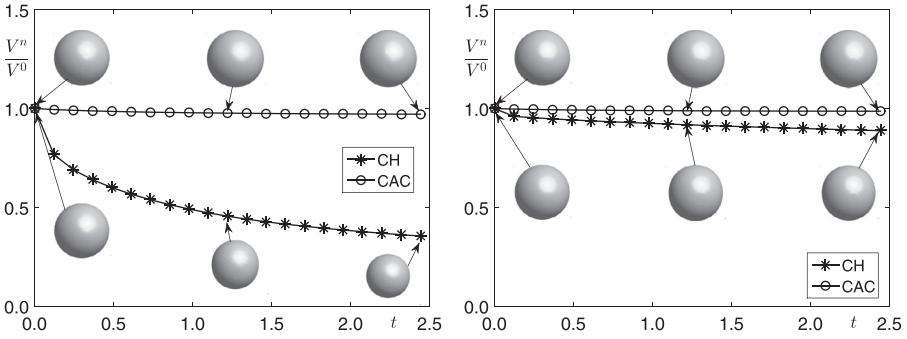

(a) $N_x = 32$ (b) $N_x = 64$

Fig. 14. Time evolution of discrete volume of a droplet in the absence of fluid flow with the CH and CAC models.

Acknowledgments

The corresponding author (J.S. Kim) was supported by Basic Science Research Program through the National Research Foundation of Korea(NRF) funded by the Ministry of Education(NRF-2016R1D1A1B03933243). The authors greatly appreciate the reviewers for their constructive comments and suggestions, which have improved the quality of this paper.

References

[1] Hua H, Shin J, Kim J. Level set, phase-field, and immersed boundary methods for two-phase fluid flows. J Fluids Eng 2014;136(2):021301.
[2] Balcázar N, Lehmkuhl O, Jofre L, Rigola J, Oliva A. A coupled volume-of-fluid/level-set method for simulation of two-phase flows on unstructured meshes. Comput Fluids 2016;124:12–29.
[3] Olsson E, Kreiss G. A conservative level set method for two phase flow. J Comput Phys 2005;210(1):225–46.
[4] Xie Y, Wodo O, Ganapathysubramanian B. Incompressible two-phase flow: diffuse interface approach for large density ratios, grid resolution study, and 3d patterned substrate wetting problem. Comput Fluids 2016;141:223–34.
[5] Shah A, Yuan L. Numerical solution of a phase field model for incompressible two-phase flows based on artificial compressibility. Comput Fluids 2011;42(1):54–61.
[6] Kumar M, Roy S. A sharp interface immersed boundary method for moving geometries with mass conservation and smooth pressure variation. Comput Fluids 2016;137:15–35.
[7] Francois M, Uzgoren E, Jackson J, Shyy W. Multigrid computations with the immersed boundary technique for multiphase flows. Int J Numer Methods H 2004;14(1):98–115.
[8] Geier M, Fakhari A, Lee T. Conservative phase-field lattice boltzmann model for interface tracking equation. Phys Rev E 2015;91(6):063309.
[9] Ren F, Song B, Sukop MC, Hu H. Improved lattice boltzmann modeling of binary flow based on the conservative allen–cahn equation. Phys Rev E 2016;94(2):023311.
[10] Inamuro T, Ogata T, Tajima S, Konishi N. A lattice boltzmann method for incompressible two-phase flows with large density differences. J Comput Phys 2004;198(2):628–44.
[11] Cahn JW, Hilliard JE. Free energy of a nonuniform system. i. interfacial free energy. J Chem Phys 1958;28(2):258–67.
[12] Badalassi VE, Ceniceros HD, Banerjee S. Computation of multiphase systems with phase field models. J Comput Phys 2003;190(2):371–97.
[13] Chella R, Vinals J. Mixing of a two-phase fluid by cavity flow. Phys Rev E 1996;53(4):3832.
[14] Ahmadlouydarab M, Azaiez J, Chen Z. Liquid bridges behavior inside microchannels subject to external pulsatile flow. Eur J Mech B Fluids 2016;57:129–42.
[15] Boyer F. A theoretical and numerical model for the study of incompressible mixture flows. Comput Fluids 2002;31(1):41–68.
[16] Jacqmin D. Calculation of two-phase navier–stokes flows using phase-field modeling. J Comput Phys 1999;155(1):96–127.
[17] Kim J. A continuous surface tension force formulation for diffuse-interface models. J Comput Phys 2005;204(2):784–804.
[18] Kim J, Kang K, Lowengrub J. Conservative multigrid methods for cahn–hilliard fluids. J Comput Phys 2004;193(2):511–43.
[19] Yang X, Feng JJ, Liu C, Shen J. Numerical simulations of jet pinching-off and drop formation using an energetic variational phase-field method. J Comput Phys 2006;218(1):417–28.
[20] Lee HG, Kim J. Two-dimensional kelvin–helmholtz instabilities of multi-component fluids. Eur J Mech B Fluids 2015;49:77–88.
[21] Kim J. Phase-field models for multi-component fluid flows. Commun Comput Phys 2012;12(03):613–61.
[22] Brassel M, Bretin E. A modified phase field approximation for mean curvature flow with conservation of the volume. Math Method Appl Sci 2011;34(10):1157–80.
[23] Kim J, Lee S, Choi Y. A conservative allen–cahn equation with a space-time dependent lagrange multiplier. Int J Eng Sci 2014;84:11–17.
[24] Gal CG, Medjo TT. On a regularized family of models for homogeneous incompressible two-phase flows. J Nonlinear Sci 2014;24(6):1033–103.
[25] Di Y, Li R, Tang T. A general moving mesh framework in 3d and its application for simulating the mixture of multi-phase flows. Commun Comput Phys 2008;3(3):582–602.
[26] Vasconcelos DFM, Rossa AL, Coutinho ALGA. A residual-based allen–cahn phase field model for the mixture of incompressible fluid flows. Int J Numer Meth Fl 2014;75(9):645–67.
[27] Chorin AJ. A numerical method for solving incompressible viscous flow problems. J Comput Phys 1997;135(2):118–25.
[28] Harlow FH, Welch JE. Numerical calculation of time-dependent viscous incompressible flow of fluid with free surface. Phys Fluids 1965;8(12):2182–9.
[29] Lee HG, Kim K, Kim J. On the long time simulation of the rayleigh–taylor instability. Int J Numer Meth Eng 2011;85(13):1633–47.
[30] Trottenberg U, Oosterlee C, Schüller A. Multigrid. London: Academic Press; 2001.
[31] Lee HG. High-order and mass conservative methods for the conservative allen–cahn equation. Comput Math Appl 2016;72(3):620–31.
[32] Sheth KS, Pozrikidis C. Effects of inertia on the deformation of liquid drops in simple shear flow. Comput Fluids 1995;24(2):101–19.
[33] Aland S, Voigt A. Benchmark computations of diffuse interface models for two-dimensional bubble dynamics. Int J Numer Meth Fl 2012;69(3):747–61.
[34] Wang Y, Shu C, Shao JY, Wu J, Niu XD. A mass-conserved diffuse interface method and its application for incompressible multiphase flows with large density ratio. J Comput Phys 2015;290:336–51.
[35] Li Y, Yun A, Lee D, Shin J, Jeong D, Kim JS. Three-dimensional volume-conserving immersed boundary model for two-phase fluid flows. Comput Methods Appl M 2013;257:36–46.